Elucidating the Ultrafast Dynamics of Photoinduced Charge Separation in Metalloporphyrin-Fullerene Dyads Across the Electromagnetic Spectrum

Zhang, J.; Pápai, Mátyás Imre; Hirsch, A.; Jennings, G.; Kurtz, C. A.; Møller, Klaus Braagaard; Lomoth, R.; Gosztola, D.; Zhang, X.; Canton, S. E.

Published in:
The Journal of Physical Chemistry Part C: Nanomaterials, Interfaces and Hard Matter

Link to article, DOI:
10.1021/acs.jpcc.6b06005

Publication date:
2016

Document Version
Peer reviewed version

Elucidating the Ultrafast Dynamics of Photoinduced Charge Separation in Metalloporphyrin-Fullerene Dyads across the Electromagnetic Spectrum

J. Zhang,[a,◊] M. Pápai,[b,c,◊] A. Hirsch,[d] G. Jennings,[e] C. S. Kurtz,[e] K. B. Møller,[b] R. Lomoth,[f] D. Gosztola,[g] X. Zhang,[e,*] and S. E. Canton[h,i,*]

Affiliations

(a) School of Environmental and Chemical Engineering, Tianjin Polytechnic University, Tianjin 300387, China
(b) Department of Chemistry, Technical University of Denmark, Kongens Lyngby DK-2800, Denmark
(c) Wigner Research Centre for Physics, Hungarian Academy of Sciences, "Lendület" (Momentum) Femtosecond Spectroscopy Research Group, P.O. Box 49, Budapest H-1525, Hungary
(d) Chair of Organic Chemistry II and Institute of Advanced Materials and Processes (ZMP), Friedrich-Alexander-Universität Erlangen-Nürnberg (FAU), Henkestrasse 42, 91054 Erlangen, Germany
(e) X-ray Sciences Division, Argonne National Laboratory, 9700 South Cass Avenue, Argonne, IL 60439, USA
(f) Department of Chemistry-Ångström Laboratory, Box 523, Uppsala University, S-75120 Uppsala, Sweden
(g) Center for Nanoscale Materials, Argonne National Laboratory, 9700 South Cass Avenue, Argonne, Illinois 60439, United States
(h) Deutsches Elecktronen Synchrotron (DESY), Notkestr. 85, Hamburg 22607, Germany
(i) Max Planck Institute for Biophysical Chemistry, Am Fassberg 11, Goettingen D-37077, Germany

Abstract

Metalloporphyrins are prominent building blocks in the synthetic toolbox of advanced photodriven molecular devices. When the central ion is paramagnetic, the relaxation pathways within the manifold of excited states are highly intricate so that unravelling the intramolecular energy and electron transfer processes is usually a very complex task. This fact is critically hampering the development of applications based on the enhanced coupling offered by the electronic exchange interaction. In this work, the dynamics of charge separation in a copper porphyrin-fullerene are studied with several complementary spectroscopic tools across the electromagnetic spectrum (from near infra-red to X-ray wavelengths), each of them providing specific diagnostics. Correlating the various rates clearly demonstrates that the lifetime of the photoinduced charge-separated state exceeds by about 10 fold that of the isolated photoexcited Cu^{II} porphyrin. As revealed by the spectral modifications in the XANES region, this stabilization is accompanied by a transient change in covalency around the Cu^{II} center, which is induced by an enhanced interaction with the C_{60} moiety. This experimental finding is further confirmed by state-of-the art calculations using DFT and TD-DFT including dispersion effects that explain the electrostatic and structural origins of this interaction, as the $Cu^{II}P$ cation becomes ruffled and approaches closer to the fullerene in the charge-separated state. From a methodological point of view, these results exemplify the potential of multielectron excitation features in transient X-ray spectra as future diagnostics of sub-femtosecond electronic dynamics. From a practical point of view, this work is paving the way for elucidating out-of-equilibrium electron transfer events coupled to magnetic interaction processes on their intrinsic time-scales.

Introduction

Combining high extinction coefficients with favorable redox properties, metalloporphyrins (MPs) take part in numerous functions essential to life, e.g. respiration or photosynthesis.[1] Their ubiquity is also related to strongly coupled electronic and geometric structures that display highly selective responsivity towards the environment. Since their physicochemical attributes are readily modulated by synthetic substitutions on the planar π-conjugated porphyrin ring and by the nature of the central

metal ion,[2,3] MPs constitute a versatile class of building blocks, which can be incorporated into Donor-Acceptor (D-A) assemblies. These molecular complexes provide a wide range of fully-functional systems for photovoltaic[4-6] and photocatalytic applications,[7] as well as biomimetic models for disentangling *in-vivo* working mechanisms.[8,9] Novel architectures are continuously being explored in order to rationalize and optimize the characteristics of the photoinduced charge gradient they can sustain.[10,11] The observations are interpreted within the framework offered by the Marcus theory of electron transfer (ET),[12,13] which casts the rates of forward and backward ET in terms of a few experimentally tunable parameters, namely the electronic coupling between the initial and the final states (H_{DA}), the driving force (i.e. the change in Gibbs free energy, $-\Delta G°$) and the reorganization energy (λ). This last component is defined as the energy dissipated for accommodating the atomic rearrangements within the bridged D-A (inner sphere, λ_i) and their solvation shells (outer sphere, λ_o). Minimizing λ has emerged as a fundamental stereochemical principle, insuring that the forward ET is close to activationless (hence very rapid), while having the backward ET in the so-called Marcus inverted exergonic region ($-\Delta G° < \lambda$), where the recombination process can slow down by orders of magnitude as the driving force increases. The 3D electron acceptors, in particular the fullerene family, hold great prospect for promoting ultrafast ET because they guarantee simultaneously low λ_i and λ_o, owing to the facile delocalization of an extra charge over the very symmetric and rigid π-conjugated cage. For example, the development of elaborate linkage modes has yielded superior MPs-C_{60} assemblies achieving near unity photoconversion efficiencies, extremely long-lived charge separation and overall λ close to that of natural photosystems.[14-19]

When containing a central metal ion with unpaired *d* electrons, such as Cu^{II}, MPs have been associated with the occurrence of energy and charge migration mediated by enhanced electromagnetic coupling.[20-26] Although this specific interaction presents definite potential, its practical utilization in photodriven molecular devices remains largely under-developed. This can be traced back to the fact that the photoinduced dynamics are complicated by the participation of (d,π), (π,d) or (d,d) charge-transfer (CT) states that have been postulated at the origin of the prompt deactivation undergone by the photoactive state. For Cu^{II}P, such CT states have usually eluded unambiguous assignment through optical and Raman spectroscopies.[27-37] Being element-specific and applicable to any state of matter, time-resolved X-ray absorption spectroscopy (TR-XAS) is a rapidly maturing technique capable of delivering unique information about the electronic and geometric structures of metastable photoexcited states with picosecond and femtosecond temporal resolution.[38-46] Recently, it has been applied as a complementary analytical tool to investigate the decay pathways in laser-excited MPs and the early steps of CO and NO ligation/deligation in heme-like porphyrins relevant for respiration.[47,48] In the present work, TR-XAS is employed in combination with ultrafast time-resolved optical absorption spectroscopy (TR-OAS) in the near infra-red and the visible regions in order to clarify the ultrafast dynamics within a prototypical Cu^{II}P following light absorption and to elucidate several unexpected aspects of the photoinduced intramolecular ET in a related Cu^{II}P-C_{60} dyad.

Materials and methods

Samples

The complexes were synthesized according to the published protocols.[49] All reagents were used as received from commercial sources without further purification.

Steady-state optical absorption spectroscopy

The UV-vis spectra were acquired on a conventional Cary spectrometer at the CNM facility of Argonne National Laboratory (USA).

Electrochemistry and spectroelectrochemistry

Electrochemical experiments were performed in a three-electrode cell using an Autolab PGSTAT302 potentiostat interfaced to a PC with GPES software (Version 4.9). A nonaqueous Ag/Ag+ electrode (CH Instruments, 0.01M AgNO3 in acetonitrile) and a glassy carbon disc electrode (3 mm diam., CH Instruments) were used as the reference and working electrode, respectively. UV-Vis spectroelectrochemical measurements were made with an Agilent 8453 diode array spectrophotometer during controlled potential electrolysis with an Autolab PGSTAT302 potentiostat. The spectroelectrochemistry cell with an optical path length of 1 mm uses a Pt mesh working electrode and the same reference electrode as described for voltammetry. All samples contained 0.1 M TBAPF6 supporting electrolyte (Fluka, electrochemical grade, dried at 80°C in vacuo) and were deaerated by purging with solvent saturated Ar and kept under Ar atmosphere during measurements.

Femtosecond Transient Absorption Spectroscopy

The TR-OAS measurements were conducted on the femtosecond laser setup used for ultrafast transient absorption spectroscopy at the CNM facility of Argonne National Laboratory (USA). The excitation beam was depolarized and set to 527 nm. For these optical measurements, the time-dependent signals were fitted to a multiexponential function, $f(t) = \sum_i A_i \exp(-t/\tau_i)$, convoluted with a Gaussian instrument response function of 120 fs fwhm.

Picosecond X-ray Absorption Spectroscopy

The TR-XAS measurements were carried out at beamline 11-ID-D of the APS (Argonne National Laboratory, USA). The optical pump pulse consisted of the second harmonic output of a Nd:YLF regenerative amplified laser at 1.6 kHz repetition rate, giving 527 nm laser pulses with 5 ps fwhm. The X-ray probe pulses with 80 ps fwhm and 6.5 MHz repetition rate were derived from the electron bunches stored in the APS ring. The two complexes were dissolved in benzonitrile (bzn) to reach 0.5 mM. This concentration ensured that the signal was not distorted by self-absorption effects (see X-ray detection below) or aggregation. The liquid sample was flowed through a stainless steel tube and formed a free jet of 550 µm diameter inside an airtight aluminum chamber. Each sample was degassed by bubbling nitrogen. The X-ray spot size was 50 µm (V) × 450 µm (H), and the laser spot was 850 µm in diameter. The X-ray and optical beams were overlapped spatially on the replenishing sample. The time delay Δt between the laser and X-ray pulses was fixed by a programmable delay line (PDL-100A-20NS, Colby Instruments) that adjusted the phase shift of the mode-lock driver for the seed laser relative to that of the RF signal of the storage ring with a precision of 500 fs. The incident X-ray energy was stepped through the Cu K edge (8988 eV) up to 700 eV above the 1s threshold. A Cu metal foil placed between two conventional ionization chambers downstream was used for X-ray energy calibration and flux monitoring purposes in transmission mode. Two avalanche photodiodes (APDs) were positioned at 90° angle on both sides of the incident X-ray beam to collect the emitted X-ray fluorescence signals. A [Soller slits/(Z-1) Ni filter] combination, which was custom-designed for the specific sample chamber configuration and the distance between the sample and the detector, was inserted between the sample jet and the APD detectors. This greatly reduced the background due to elastic X-ray scattering. An additional APD was employed to monitor the intensity of the incident X-ray beam. The outputs of the APDs were sent to two fast analyzer cards (Agilent) that were triggered by a signal at 1.6 kHz from the scattered laser light onto a photodiode. The card digitized the X-ray fluorescence signals as a function of time at 1 ns/point after each trigger. The fluorescence signals from the synchronized X-ray pulse at a 100 ps delay after the laser pump pulse excitation were accumulated to build the XAS trace μ_{laser_ON}. The fluorescence signals from the same X-ray pulse averaged over 50 round trips in the storage ring prior to the laser pulse were recorded to

build the corresponding XAS trace μ_{laser_OFF}. With this collection scheme, the μ_{laser_ON} and μ_{laser_OFF} data were taken under the exact same experimental conditions for sample, laser, and beamline, with the shot-to-shot normalization of the X-ray pulse intensities performed by the acquisition software. This allowed canceling out any error associated with drifts. Analyzing the difference signal $\Delta\mu = [\mu_{laser\_ON} - \mu_{laser\_OFF}]$ originating from the fraction α of molecules in the excited state delivers the XA spectrum of the photoexcited complexes. The integrity of the sample over time was checked by comparing from scan to scan the line shapes of the XASz trace μ_{laser_OFF} in the XANES region. No change due to radiation damage could be detected throughout the duration of the experiment.

Results and discussion

Spectroscopic characterizations of $Cu^{II}P$ and $Cu^{II}P$-C_{60} in their ground state.

The chemical structures of the $Cu^{II}P$ and $Cu^{II}P$-C_{60} are given in Figure 1a and 1b. The dyad was obtained through the tether directed remote functionalization strategy.[49] The two-point attachment maintains the components into a van der Waals π stack (~ 3 Å). The electrochemistry measurements are shown in Figure S1. The redox potentials of the two complexes dissolved in benzonitrile (bzn) are given in Table S1. The oxidation of $Cu^{II}P$ has basically the same potential in the dyad, while its reduction presents a somewhat more negative potential due to the fact that C_{60} moiety is inevitably reduced before.

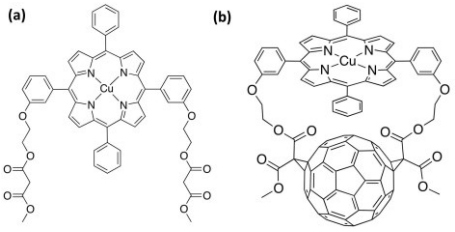

Figure 1. Chemical structure of (a) $Cu^{II}P$ and (b) $Cu^{II}P$-C_{60}.

The electronic structure of MPs is well-described by the so-called 4-orbital model.[50,51] In the free-base porphyrin π–conjugated macrocycle of D_{4h} symmetry, promotion from the closely spaced $a_{2u}(\pi)$ and $a_{1u}(\pi)$ HOMOS into the $e_g(\pi^*)$ LUMO populates two quasi-degenerate singlet excited states $^1(\pi,\pi^*)$ that are subject to configuration interaction. This leads to the Soret band ($^2S_2$) with very large oscillator strength in the near UV and to the weaker Q band ($^2S_1$) lying in the visible. The optical absorption spectra of $Cu^{II}P$ and $Cu^{II}P$-C_{60} in bzn are displayed in Figure 2a, which focusses on the range covering the Q bands (500-600 nm). Identical spectra are measured in non-coordinating toluene, establishing that the complexes in their ground states are not affected by any ligation with solvent molecules (**Figure S2**). A small red shift of ~ 3 nm is observed for the Q bands of $Cu^{II}P$-C_{60} relatively to $Cu^{II}P$. This can be attributed to the weak van der Waals interaction between the porphyrin and the fullerene.

The geometries of the $Cu^{II}P$ and $Cu^{II}P$-C_{60} in bzn were optimized with DFT including dispersion effects (S3 contains the computational details). Their absorbance in UV-vis region were simulated with TD-DFT. They are shown in Figure 2b along with the dominant transitions (Table S2). These calculations not only capture the intensity redistribution in the Soret band, but also the red shift of the Q band in $Cu^{II}P$-C_{60} (~ 5nm) that could only be reproduced when considering the dispersion effects (Figure S3).

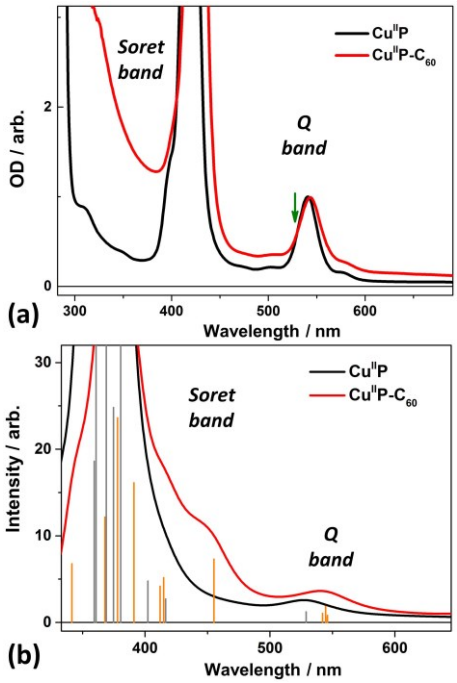

Figure 2. (a) UV-vis spectra of $Cu^{II}P$ (grey) and $Cu^{II}P$-C_{60} (red) in bzn, normalized at the maximum of the Q band. The arrow indicates the excitation laser wavelength used in all the pump-probe measurements. (b) Absorbance of $Cu^{II}P$ (black) and $Cu^{II}P$-C_{60} (red) modelled with TD-DFT. The dominant contributions are indicated with grey and orange sticks respectively.

Further insight into the subtle coupling between the porphyrin and the fullerene can be obtained by inspecting their X-ray absorption spectra at the Cu K edge, which originate from 1s core ionization. The normalized X-ray absorption coefficients μ of $Cu^{II}P$ and $Cu^{II}P$-C_{60} are shown in Figure 3a. Both exhibit the typical features of quasi-planar 4-coordinated Cu^{II} compounds (see inset of Figure 3a). The weak pre-edge at 8.979 keV arises from the quadrupole-allowed $1s \rightarrow 3d$ transition, which is only prominent in absence of inversion symmetry.[52,53] The shoulder M_1 at 8.992 eV and the peak M_2 at 8.997 eV are assigned respectively to the $1s \rightarrow 4pz$ and to the $1s \rightarrow 4px,y$ transitions. The broad peak B around 9 eV is caused by multiple scattering of the photoelectron within the first coordination shell of Cu^{II} [54,55] so that its energy position indirectly depends upon the Cu^{II}-N bond length. Long under debate, the assignment of peak S at 8.985 keV was eventually ascertained through polarization-resolved XAS experiments[56] and *ab-initio* calculations.[57-60] It is now accepted as being associated to the dipole-allowed promotion of a core electron to a molecular state with primary configuration ($1s^1 3d^{10} 4p^1 L^0$) where *L* is the ligand orbital.[61-67] In this relaxed state, the core hole is stabilized through additional screening due to partial charge transfer from the ligand orbital *L* to the half-filled metal orbital $3dx^2\text{-}y^2$, a process generally known as shakedown. This transition denoted $1s \rightarrow 4p$+*shakedown* is a sensitive fingerprint for any modification in the covalency of the metal-ligand bond. [61-67] Specifically, when a molecular complex experiences a decrease in bond covalency, e.g. when the spatial overlap between the *d* and *L* energy levels diminishes, the charge transfer from the ligand to the metal occurs less efficiently, hence the shakedown process becomes less probable and the energy separation between M_1 and S decreases.[64-68] Consequently, a relative shift of S to higher photon energy directly reflects a decrease in bond covalency. Figure 3b (blue trace) shows the difference spectrum between the static X-ray absorption coefficients of $Cu^{II}P$-C_{60} and $Cu^{II}P$ acquired under the same experimental conditions. The distinct shift of the shakedown peak S to higher photon energy pinpoints an alteration in metal-ring covalency induced by the weak axial interaction with the bulky fullerene: the half-filled $3dx^2\text{-}y^2$ is stabilized, while the filled $3dz^2$ is destabilized (see inset of Figure 3a and Figure 3b). As a result, the overlap between $3dx^2\text{-}y^2$ and *L*

decreases, hence as outlined above, S is now located at higher energy for $Cu^{II}P$-C_{60}. Concurrently, the reduction of the covalent character within the equatorial plane stabilizes the in-plane *4px,y* component and destabilizes the out-of-plane *4pz* component, which is in line with peaks M_2 and M_3 shifting respectively to slightly lower and higher energies. Finally, the change in covalency also translates into a small Cu-N bond elongation, with the multiple-scattering peak B moving to lower energy.[54,55] This is confirmed by a preliminary analysis Fourier transform of the extended X-ray absorption fine structure (EXAFS) oscillation R. The experimental observations are all supported by the results of the DFT calculations that include empirically the dispersion effects used for the FEFF9.0 simulations of the difference profile shown in Figure 3b (orange trace). The non-structural parameters introduced in the XANES simulations have been benchmarked for Cu^{II} poprhyrins.

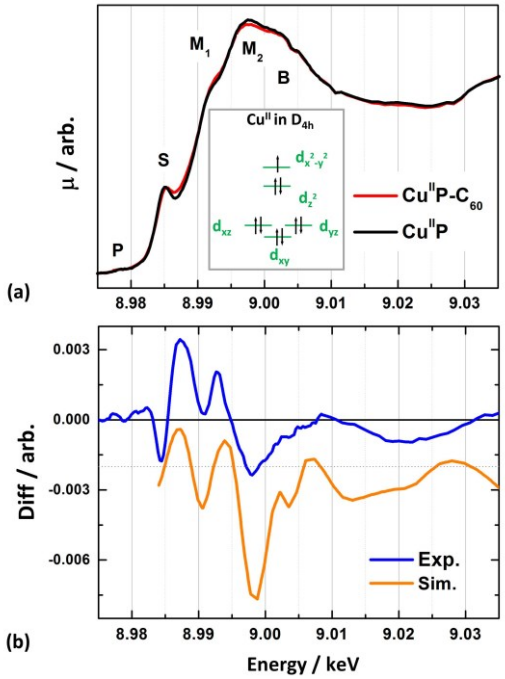

Figure 3. (a) $Cu^{II}P$ (black trace) $Cu^{II}P$-C_{60} (red trace) in bzn. (b) Difference (blue trace) and simulated from FEFF9.0 simulations and calculated DFT structures (orange trace). The inset shows the splitting of the 3d levels of Cu^{II} in a D_{4h} ligand field.

Figure 4a and 4b present these DFT optimized geometries, where a deformation in the planar π-conjugated ring of $Cu^{II}P$ can be observed for the dyad. The average Cu-N bond lengths are given in Table S4. Including the dispersion effects in the optimization is crucial to capture the structural details of these large molecular complexes, such as the bond elongation in the dyad, or the proximity of the porphyrin and the fullerene, which is manifested by a Cu-C bond distance close to that of a chemical bond (i.e. here 2.6 Å). The resulting weak electronic communication can be viewed by examining the frontier orbitals of $Cu^{II}P$ and $Cu^{II}P$-C_{60} displayed in Figure 4c and 4d. Whereas the HOMOs are similar in both complexes, the LUMO has a clear mixed porphyrin-fullerene character, indicating some degree of electronic delocalization.

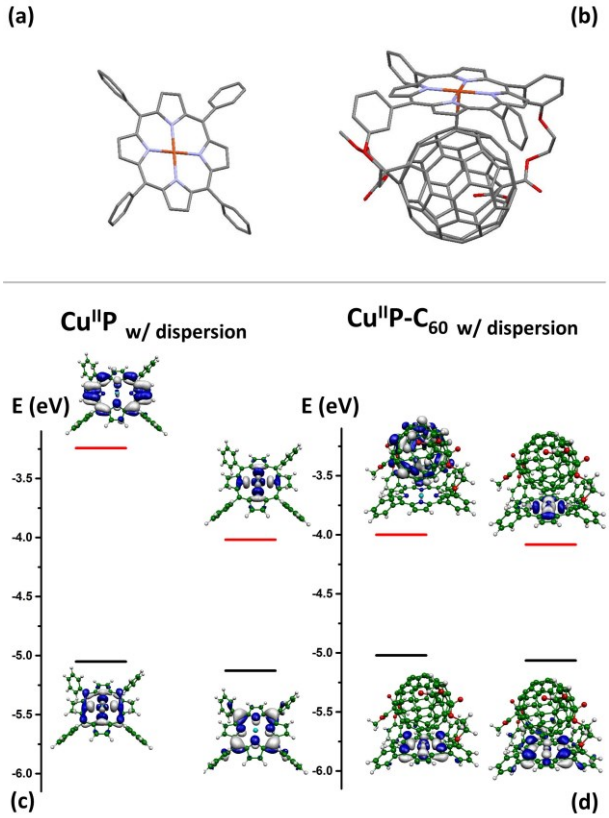

Figure 4. DFT optimized structures of (a) $Cu^{II}P$ and (b) $Cu^{II}P$-C_{60} with explicit introduction of dispersion effects. The H atoms have been omitted for clarity. Corresponding spin-up and spin-down frontier orbitals for (c) $Cu^{II}P$ and (d) $Cu^{II}P$-C_{60}.

To summarize, the specific markers of the van der Waals interaction between the porphyrin moiety and the close-lying fullerene in the $Cu^{II}P$-C_{60} dyad have been identified in the lineshapes of the optical and X-ray absorption spectra, in agreement with DFT and TD-DFT calculations. They can now be followed in real time to obtain some information about the photoinduced processes in the chromophore and the linked complex.

Ultrafast spectroscopic characterization of photoexcited $Cu^{II}P$ and $Cu^{II}P$-C_{60}

Ultrafast spectroscopic measurements were carried out with several pump-probe detection schemes in order to track the photoinduced dynamics in $Cu^{II}P$ and $Cu^{II}P$-C_{60}. Figure 5a, 5b, 5c and 5d contain the representative results from TR-OAS.

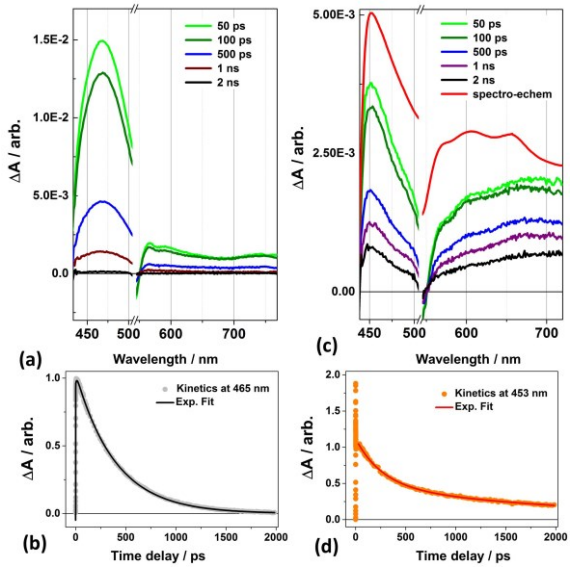

Figure 5. (a) TR-OAS after 527 nm excitation for $Cu^{II}P$ in bzn. (b) Kinetics acquired at 465 nm for $Cu^{II}P$ in bzn. (c) TR-OAS after 527 nm excitation for $Cu^{II}P$-C_{60} in bzn. (d) Kinetics acquired at 453 nm for $Cu^{II}P$-C_{60} in bzn

Figure 5a displays the expected transient optical absorption spectra of $Cu^{II}P$ in bzn after laser excitation at 527 nm.[29,37,64-66] In the presence of the paramagnetic Cu^{II} metal ion, the exchange interaction between the electrons occupying the half-filled $3dx^2$-y^2 and the $^{1,3}(\pi,\pi)^*$ ring states acts as a perturbation, which modifies the energy levels: the singlet states become singdoublets (^2S), while the triplets split into the weakly luminescent tripdoublet (^2T) and tripquartet (^4T) states in Boltzmann equilibrium (Figure 6).

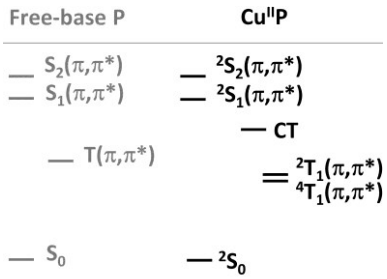

Figure 6. Sketch illustrating the perturbation introduced on the energy levels of the free base porphyrin P by the Cu^{II} cation in $Cu^{II}P$.

Femtosecond laser spectroscopy has delivered 30 fs as the upper limit for the decay of the initially excited $^2S_1$ to the trip manifold via intersystem crossing (ISC).[37] In non-coordinating solvents, e.g. toluene, the vibrationally equilibrated trip population decays directly back to the ground state over a few nanoseconds. In nitrogen-containing Lewis base solvents, such as bzn, it is instead quenched within about a hundred of picoseconds.[30-34] Figure5b shows the kinetics at 465 nm, which can be fitted with a single-exponential decay lifetime of 396 ± 5 ps. The trends in lifetime reduction have been convincingly explained by solvent-dependant energetics of the CT states. Weak axial coordination of a bzn molecule stabilizes the particular excited CT state of $Cu^{II}P$ whose energetics are directly influenced by the Cu…Naxial separation, opening up a new channel in the reversible photocycle (Figure 7).

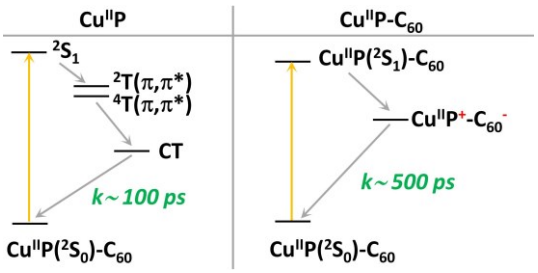

Figure 7. Jablonksi diagram for $Cu^{II}P$ (left) and $Cu^{II}P$-C_{60} (right) in bzn.

However, the exact assignment remains partly tentative to date since the CT state is too short-lived to be unambiguously identified by transient resonant Raman spectroscopy.[30,34] In addition, various theoretical models do not concord yet in their predictions, either for its identity or for its energy position.[57,60] Figure 5c shows the transient optical absorption spectra of $Cu^{II}P$-C_{60} in bzn for several pump-probe time delays after initial laser excitation at 527 nm. The transient signal in the visible displays significantly longer lifetime compared to $Cu^{II}P$ (Figure 5a). The intricate early dynamics proceed out of equilibrium with highly non-single exponential behaviour. Nevertheless, after ~10 ps, the lineshape resembles the difference spectrum of the oxidized species $Cu^{II}P^{+}$-C_{60} created independently through spectroelectrochemistry. As such, the kinetics at 453 nm (Figure 5d) follow the lifetime of the charge separated state through the P cation signal. The trace can be fitted with two single-exponential, yielding 328 ±13 ps and 3066 ± 150 ps as time constants. In the near IR region, a band is clearly detected at ~1040 nm. It is the known signature of the C_{60}^{-} anion and therefore the extracted kinetics at 1040 nm pinpoint the arrival of the electron at the fullerene moiety.[69] The time constants in the near IR (384 ± 60 ps and 3340 ± 676 ps) match the ones observed in the visible (Figure 8).

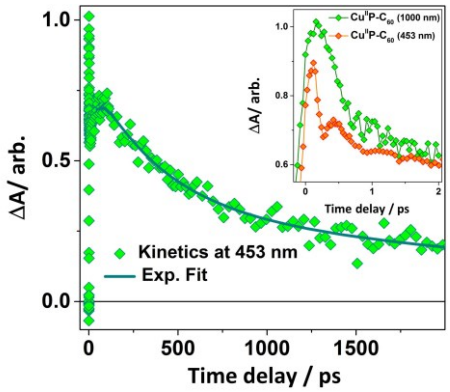

Figure 8. Kinetics extracted at 900 nm for $Cu^{II}P$-C_{60} (green) and $Cu^{II}P$ (grey). The inset zooms on the early time scales.

It could be noted here that the oscillatory behavior in the visible covers the time span for the appearance of the electron signal at the C_{60} (inset of Figure 8). These early out of equilibrium dynamics will be studied as a function of incident wavelength and solvent in upcoming work. In contrast, no signal arises at 900 nm for $Cu^{II}P$ (grey trace in Figure 8). Collectively, these spectroscopic observations reveal that, unexpectedly, the dyad can sustain a long-lived charge separated state (over >700 ps) despite the rapid deactivation found in the isolated chromophore $Cu^{II}P$. All the time scales are summarized in Table S5.

TR- XAS with 80 ps temporal resolution was then employed to track the dynamical evolution of the element specific core-shell transition that involves a Cu 1s electron. This technique enables visualizing the coupled electronic and structural changes that accompany the quenching of the $Cu^{II}P$

(^{2,4}T) in the isolated moiety and the stabilization the CS state in the dyad with atomic selectivity. Figure 9 (left) shows the transient difference spectrum $\mu_{laser\_ON} - \mu_{laser\_OFF}$ for $Cu^{II}P$ in bzn around the shakedown peak in the near-edge region at a pump-probe delay of 100 ps. The extremely low concentration employed in this experiment (i.e. 0.5 mMol) was crucial to rule out any possible aggregation between the solvated chromophores, as this effect is known to have a profound impact on the lifetimes and the deactivation pathways of the excited species. At the sensitivity level of the experiment, a distinct decrease of the shakedown intensity can be observed. Following excitation in the $^2S_1$ Q band, the population decays to the ^{2,4}T very rapidly. This state is expected to undergo a slight Cu-N elongation because the $e_g(\pi*)$ LUMO is antibonding and the $a_{2u}(\pi)$ HOMO exhibits large electron density at the N_{pyrole} and the C_{meso} (Figure 4c).[36] It presents then a greater affinity towards ligation than the ground state. The tendency for axial coordination of a bzn molecule to induce a symmetry lowering towards C_{4v}, with out-of-plane metal displacement (i.e. doming) favors the $a_{2u}(\pi)$-$3dx^2$-y^2 interaction, hence the concurrent formation of a (π,d) CT state with bond lengthening. This is in line with the decreased intensity of the S shakedown feature since the $3dx^2$-y^2 gains electron density from the ring through intramolecular electronic redistribution. Another possible signature for (π,d) CT formation would be the decrease of the *1s* $\rightarrow$ *3d* pre-edge oscillator strength, but the signal to noise (S/N) ratio achievable in this experiment with sub mMol concentration was insufficient in this spectral range.

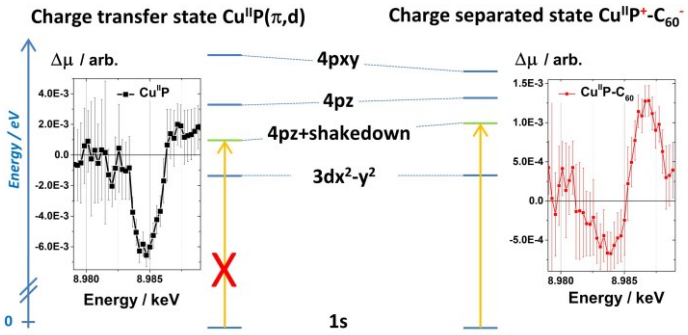

Figure 9. Transient X-ray signal in the vicinity of the *1s* $\rightarrow$ *4pz+shakedown* transition for $Cu^{II}P$ (black) and $Cu^{II}P$-C_{60} (red).

Finally, considering the dyad, photoabsorption triggers charge separation as described above. The difference spectrum $\mu_{laser\_ON} - \mu_{laser\_OFF}$ for $Cu^{II}P$-C_{60} in bzn reveals a shift to higher energy for the shakedown peak as seen in Figure 9 (right). Since the concentration (i.e. 0.5 mMol) and the extinction coefficients at 527 nm are similar, while the X-ray and laser parameters (spot size and incident flux) were kept unchanged, the differences between $Cu^{II}P$ and $Cu^{II}P$-C_{60} cannot be due to variations in experimental conditions. The transient change of covalency observed for $Cu^{II}P$-C_{60} is reminiscent of the one displayed in Figure 2. The trend can be ascribed to the effective oxidation of the ring orbital and to the closer approach of the fullerene, with a Cu-C now of 2.533 Å as predicted by DFT (Figure 10a and Figure b).

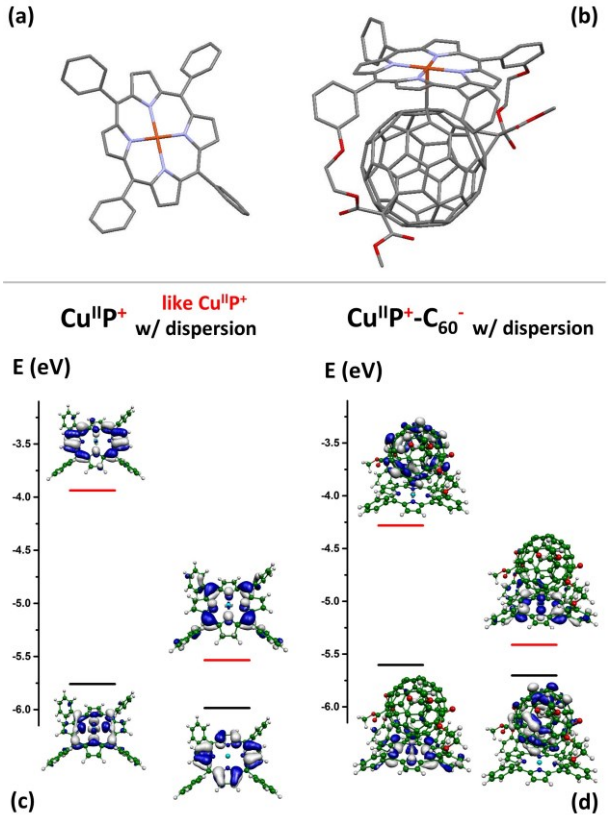

Figure 10. DFT optimized structures of (a) $Cu^{II}P^{+}$ and (b) $Cu^{II}P^{+}$-C_{60}^{-} with explicit introduction of dispersion effects. The H atoms have been omitted for clarity. Corresponding spin-up and spin-down frontier orbitals for (c) $Cu^{II}P^{+}$ and (d) $Cu^{II}P^{+}$-C_{60}^{-}.

Upcoming TR-XAS experiments with higher S/N will be attempted next, in order to ascertain experimentally the predicted structural changes of a few picometers (Table S6), a task which remains demanding in the sub-millimolar regime.[70,71] It should be noted that the transient change in covalency revealed by the optical pump-X-ray probe measurement could also be affected by the coupling between the unpaired metal electrons and the ring electrons. In any non-D_{4h} structure, the spatial overlap between *3dx2-y*^{2} and $a_{2u}(\pi)$ is significant enough for the spins to couple antiferromagentically, a phenomenon recognized as conceptually undistinguishable from bond formation.[72,73] This points out to a definite role of an intracomponent exchange interaction during the ultrafast ET within this type of molecular assembly. An accurate modelling of these effects will prove demanding since it will require taking into account simultaneously the partial delocalization of the LUMO over the two moieties (Figure 10c and Figure 10d) as well as the through- space van der Waals $\pi-\pi$ interactions which are strongly affected by the solvent, both in the ground and excited states. As the core-shell transition involves localized Cu^{II} orbitals, electronic relaxation is important and multielectron effects, such as the shakedown process, need to be benchmarked and included in order to unravel the ultrafast dynamics. Because these weak features are known to be difficult to pinpoint solely through K edge XAS, complementary support from transient L edge XAS in the soft X-ray regime,[74,75] from transient valence to core X-ray emission[76-78] and from future transient resonant X-ray Raman spectroscopy[79,80] would also be valuable to unambiguously disentangle the spin, electronic and structural information, and to eventually build a complete understanding of the mechanisms at play. With the development of advanced spectroscopic tools gathering and correlating complementary diagnostics across the electromagnetic spectrum, it is now possible to draw exhaustive maps for the pathways of energy and electron migration within large chromophore-fullerene assemblies. In the near future, this generalized methodology will be applied to the most challenging but highly promising aspects of hot ET in this important class of photoactive donor-

acceptor systems, such as controlling directionality,[81-83] utilizing exciplex mediation,[84-86] or activating multi-step charge separation.[87]

Conclusion

In conclusion, this work follows the dynamics of charge separation in a porphyrin and a related porphyrin-fullerene dyad with ultrafast spectroscopies, from the near IR to the X-ray regime. It provides a detailed correlation between the various timescales, hence a unified description of this fundamental process. While the kinetics in the UV visible track the evolution in the $Cu^{II}P$ cation, the kinetics in the near IR provide a unique fingerprint of the electronic localization at the fullerene site. In the hard X-ray regime, the kinetics clarify the decay pathway of the isolated $Cu^{II}P$ chromophore via an optically-dark (π,d) charge-transfer state stabilized through axial interaction with a bzn molecule. The X-ray diagnostic complements the conventional TR-OAS measurements by revealing that the origin of the charge stabilization is an increased interaction between the $Cu^{II}P$ cation and the fullerene. Uncovering the possible role of the magnetic coupling between the unpaired electron on the Cu^{II} center and the hole in the porphyrin will be attempted with time-resolved XES. With the rapid increase in reachable S/N, the study of the EXAFS region will be undertaken to extract the minute changes in bond lengths that are nevertheless crucial to eventually understand molecular and biological magnetism. This work also shows that the rationalization of the structural trends for anions and cations of MP which are highly complicated by the interaction can now be pursued. More generally, these results demonstrate that it is possible to incorporate paramagnetic porphyrins in D-A assemblies despite the short excited state lifetime of the isolated chromophore. In the present work, the charge separated state lifetime in $Cu^{II}P$-C_{60} exceeds that of the photoexcited MP moiety by about 10 fold. The out of equilibrium nature of the charge separation can be studied at XFEL sources. From a methodological point of view, this work pinpoints the need for developing further of the understanding of multiple electron effects on the XANES region, such as the shakedown in the present study. As illustrated in this work, these processes represent very fine spectral signatures of covalency changes. Since they originate from electron-electron correlations, they are inherently susceptible to sub-femtosecond resolution. Finally, this work is paving the way for the elaboration of novel design strategies, wherein magnetic coupling can complement the well-studied electronic coupling towards optimize the rates of charge transfer within functional molecular devices.

Supporting Information

Cyclic voltammograms, Redox potentials, UV-vis spectra, Computational details, Table of main optical transitions for the Cu porphyrin, Table of main optical transitions for the dyad, TD-DFT UV-vis spectra without dispersion, Table of Cu-N bond lengths in the Cu porphyrin, Table of TR-OAS time constants, Table of Cu-N bond elongation in the dyad.

Acknowledgements

J. Z. greatly acknowledges support from NSFC (21302138) and Tianjin City High School Science and Technology Fund Planning Project (20130504). M. Ruppert is greatly acknowledged for her contribution in the early part of the project. The research leading to the presented results has received funding from the People Program (Marie Curie Actions) of the European Union's Seventh Framework Program (FP7/2007-2013) under REA grant agreement n° 609405 (COFUNDPostdocDTU) to M. P. X. Z., the use of the Advanced Photon Source and the Center for Nanoscale Materials were supported by the U.S. Department of Energy, Office of Science, Office of Basic Energy Sciences, under Contract No. DE-AC02-06CH11357. S. E. C. acknowledges funding from SFB 1073.

Notes for authorlist

[◊] These authors contributed equally to the work

Contact information for corresponding authors

Sophie. E. Canton:
Email: sophie.canton@desy.de
Tel:00-49-40 8998-4718
Xiaoyi Zhang:
Email: xyzhang@aps.anl.gov
Tel: 00-1-630-252-0366

References

[1] Cook, S. A.; Hill, E. A.; Borovik, A. S. Lessons from Nature: A Bio-Inspired Approach to Molecular Design. *Biochemistry* **2015**, *54*, 4167-4180.

[2] Shelnutt, J. A.; Song, X. Z.; Ma, J. G.; Jia, S. L.; Jentzen, W.; Medforth, C. J. Nonplanar Porphyrins and their Significance in Proteins. *Chem. Soc. Rev.* **1998**, 27, 31-42.

[3] de la Torre, G.; Bottari, G.; Sekita, M.; Hausmann, A.; Guldi, D. M. A Voyage into the Synthesis and Photophysics of Homo- and Heterobinuclear Ensembles of Phthalocyanines and Porphyrins. *Chem. Soc. Rev.* **2013**, *42*, 8049-8105.

[4] Jurow, M. Schuckman, A. E.; Batteas, J. D.; Drain, C. M. Porphyrins as Molecular Electronic Components of Fuctional Devices. *Coord. Chem. Rev.* **2010**, *254*, 2297-2310.

[5] Higashino, T.; Imahori, H. Porphyrins as Excellent Dyes for Dye-sensitized Solar Cells: Recent Developments and Insights. *Dalton Trans.* **2015**, *44*, 448-463.

[6] Panda, M. K.; Ladomenou, K.; Coutsolelos, A. G. Porphyrins in Bio-Inspired Transformations: Light-harvesting to Solar Cell. *Coord. Chem. Rev.* **2012**, *256*, 2601-2627.

[7] Ladomenou, K.; Natali, M.; Iengo, E.; Charalampidis, G.; Scandola, F.; Coutsolelos, A. G. Photochemical Hydrogen Generation with Porphyrin-based Systems. *Coord. Chem. Rev.* **2015**, *304*, 38-54.

[8] Pratviel, G. Porphyrins in Complex with DNA: Modes of Interaction and Oxidation Reactions. *Coord. Chem. Rev.* **2016**, *308*, 460-477.

[9] Simoes, M. M. Q.; Neves, C. M. B.; Pires, S. M. G ; Neves, M. G. P. M. S.; Cavaleiro, J. A. S. Mimicking P_{450} Process and the Use of Metalloporphyrins. *Pure Appl. Chem.* **2013**, *85*, 1671-1681.

[10] Kilså, K.; Kajanus, J.; Macpherson, A. N.; Mårtensson, J.; Albinsson, B. Bridge-Dependent Electron Transfer in Porphyrin-Based Donor-Bridge-Acceptor Systems. *J. Am. Chem. Soc.* **2001**, *123*,

3069-3080.

[11] Andersson, M.; Linke, M.; Chambron, J.-C.; Davidsson, J.; Heitz, V.; Hammarström, L.; Sauvage, J. P. Long-Range Electron Transfer in Porphyrin-Containing [2]-Rotaxanes: Tuning the Rate by Metal Cation Coordination. *J. Am. Chem. Soc*. **2002**, *124*, 4347-4362.

[12] Schuster, D. I.; Cheng, P.; Jarowski, P.D.; Guldi, D. M.; Luo, C. P.; Echegoyen, L.; Pyo, S.; Holzwarth, A.R.; Braslavsky, S.E.; Williams, R.M.; Klihm, G. Design, Synthesis, and Photophysical Studies of a Porphyrin-Fullerene Dyad with Parachute Topology; Charge Recombination in the Marcus Inverted Region. *J. Am. Chem. Soc.* **2004**, *126*, 7257-7270.

[13] Imahori, H.; Tamaki, K.; Guldi, D. M.; Luo, C. P.; Fujitsuka, M.; Ito, O.; Sakata, Y.; Fukuzumi, S. Modulating Charge Separation and Charge Recombination Dynamics in Porphyrin−Fullerene Linked Dyads and Triads: Marcus-Normal versus Inverted Region. *J. Am. Chem. Soc.* **2001**, *123*, 2607-2617.

[14] Araki, Y.; Ito, O. Factors controlling lifetimes of photoinduced charge-separated states of fullerene-donor molecular systems. *J. Chem. Photochem. Photobiol. C* **2008**, *9*, 93-110

[15] Guldi, D. M.;Illescas, B. M.; Atienza, C. M.; Wielopolskia, M.; Martin, N. Fullerene for Organic Electronics. *Chem. Soc. Rev.* **2009**, *38*, 1587-1597.

[16] Higashino, T.; Yamada, T; Yamamoto, M. ; Furube, A.; Tkachenko, N.V .; Miura, T. ; Kobori, Y. ; Jono, R.; Yamashita, K. Remarkable Dependence of the Final Charge Separation Efficiency on the Donor-Acceptor Interaction in Photoinduced Electron Transfer. *Angew. Chem. Int. Ed.* **2016**, *55*, 629-633.

[17] Kirner, S.V.; Henkel, C.; Guldi, D. M.; Megiatto, J. D.; Schuster, D. I. Multistep Energy and Electron Transfer Process in Novel Rotaxane Donor-acceptor Hybrids Generating Microsecond-lived Charge Separated States. *Chem. Sci.* **2015**, *6*, 7293-7304.

[18] Konev, A. S.; Khlebnikov, A. F; Prolubnikov, P. I.; Mereshchenko, A. S.; Povolotskiy, A. V.; Levin, O. V.; Hirsch, A. Synthesis of New Porphyrin-Fullerene Dyads Capable of Forming Charge-Separated States on a Microsecond Lifetime Scale. *Chem.-Eur. J.* **2015**, 21, 1237-1250.

[19] Schuster, D. I.; Loa, K.; Guldi, D. M.; Palkar, A.; Echegoyen, L.; Stanisky, C.; Cross, R. J.; Niemi, M.; Tkachenko, N. V. Azobenzene-Linked Porphyrin−Fullerene Dyads. *J. Am. Chem. Soc.*

2007, *129* ,15973-15982.

[20] Guldi, D. M.; Nuber, B.; Bracher, P. J.; Alabi, C. A; MacMahon, S; Kukol, J. W.; Wilson, S. R.; Schuster, D. I. Synthesis and Photophysics of a Copper-Porphyrin-Styrene-C_{60} Hybrid. *J. Phys. Chem. A* **2003**, *107*, 3215-3221.

[21]Pettersson, K.; Kilsa, K.; Martensson, A.; Albinsson, B. Intersystem Crossing versus Electron Transfer in Porphyrin-Based Donor−Bridge−Acceptor Systems: Influence of a Paramagnetic Species. *J. Am. Chem. Soc.* **2004**, *126*, 6710-6719.

[22] Yoon, H.; Lim, J.; Gee. H.-C.; Lee, C.-W.; Jeong, Y.-W.; Kim, D.; Jang, W.-D. A Porphyrin-Based Molecular Tweezer: Guest-Induced Switching of Forward and Backward Photoinduced Energy Transfer. *J. Am. Chem. Soc.* **2014**, *136*, 1672-1679.

[23] Asano-Someda, M.; Kaizu, Y. Highly Efficient Triplet−Triplet Intramolecular Energy Transfer and Enhanced Intersystem Crossing in Rigidly Linked Copper(II) Porphyrin−Free Base Porphyrin Hybrid Dimers. *Inorg. Chem.* **1999**, *38*, 2303-2311.

[24] Toyama, N.; Asano-Someda, M.; Ichino, T; Kaizu, Y. Enhanced Intersystem Crossing in Gable-Type Copper(II) Porphyrin−Free Base Porphyrin Dimers: Evidence of Through-Bond Exchange Interaction. *J. Phys. Chem. A* **2000**, *104*, 4857-4865.

[25] Hay, S.; Smith, T. A.; Ghiggino, K.P.; Wydrzynski, T. *Proc. Nat. Acad. Sci.* USA **2004**, 101, 17675-17680.

[26] Grinstaff, M. W.; Hill, M. G.; Labinger, J. A.; Gray, H. B. Mechanism of Catalytic Oxygenation of Alkanes by Halogenated Iron Porphyrins. *Science* **1994**, *264*, 1311-1313.

[27] Asano- Someda, M.; Aoyagi, K.; Kitagawa, T. Time-resolved Resonance Raman Spectra of Octaethylporphinato Copper(II) in the Lowest Excited Triplet State. *Chem. Phys. Lett.* **1996**, 257, 492-498.

[28] Sato, S.; Asano-Someda, M.; Kitagawa, T. Time-resolved Resonance Raman Spectra of Free-base Octaethylporphyrin in the S_1 and T_1 States. *Chem. Phys. Lett*. **1992**, 189, 443-447.

[29] Magde, D.; Windsor, M. W.; Holten, D.; Gouterman, M.Piosecond Flash Photolysis: Transient Absorption in Sn(IV), Pd(II), and Cu(II) Porphyrins. *Chem. Phys. Lett.* **1974**, *29*, 183-188.

[30] dePaula, J. C.; Walters, V. A.; Jackson, B. A.; Cardozo, K. Transient Resonance Raman Spectroscopy of Copper(II) Complexes of meso-tetraphenylporphine and meso-tetraphenylchlorin. *J. Phys. Chem.* **1995**, *99*, 4373-4379.

[31] Jeoung, S. C.; Kim, D.; Cho, D. W.; Yoon, M. Time-Resolved Resonance Raman Spectroscopic Study on Copper(II) Porphyrins in Various Solvents: Solvent Effects on the Charge Transfer States. *J. Phys. Chem*. **1995**, *99*, 5826-5833.

[32] Jeoung, S. C.; Kim, D.; Cho, D. W.; Yoon, M. Time-Resolved Resonance Raman and Transient Absorption Studies on Water-Soluble Copper(II) Porphyrins. *J. Phys. Chem*. **1996**, *100*, 3075-3083.

[33] Jeoung, S. C.; Eom, H. S.; Kim, D.; Cho, D. W.; Yoon, M. Exciplex Formation Dynamics of Photoexcited Copper(II) Tetrakis(4-*N*-methylpyridyl)porphyrin with Synthetic Polynucleotides Probed by Transient Absorption and Raman Spectroscopic Techniques. *J. Phys, Chem. A* **1997**, *101*, 5412-5417.

[34] Kruglik, S. G.; Apanasevich, P. A.; Chirnovy, V. S.; Kvach, V. V.; Orlovich, V. A. Resonance Raman, CARS, and Picosecond Absorption Spectroscopy of Copper Porphyrins: The Evidence for the Exciplex Formation with Oxygen-Containing Solvent Molecules. *J. Phys. Chem.* **1995**, *99*, 2978-2995.

[35] Aronowitz, Y. J.; Gouterman, M. Effect of Metal and Substituents on the Quasi-line Spectra of Some Metalloporphyrins. *J. Mol. Spec*. **1977**, *64*, 267-289.

[36] Czernuszewicz, R.; Maco, K. A.; Li, X. Y.; Kincaid, J. R.; Spiro, T. G. Resonance Raman Spectroscopy Reveals a1u vs. a2u Character and Pseudo-Jahn-Teller Distortion in Radical Cations of Nickel(II), Copper(II), and Chloroiron(III) Octaethyl- and Tetraphenylporphyrins. *J. Am. Chem. Soc.* **1989**, *111*, 3860-3869.

[37] Kim, D.; Holten, D.; Gouterman, M. Evidence from Picosecond Transient Absorption and Kinetic Studies of Charge-transfer States in Copper(II) Porphyrins. *J. Am. Chem. Soc*. **1984**, *106*, 2793-2798.

[38] Shelby, M. L.; Mara, M. W.; Chen, L. X. New Insight into Metalloporphyrin Excited State Structures and Axial Ligand Binding from X-ray Transient Absorption Spectroscopic Studies. *Coord. Chem. Rev.* **2014**, *277*, 291-299.

[39] Chen, L. X.; Zhang, X. Y; Wasinger, E. C.; Lockard, J. V.; Stickrath, A. B.; Mara, M. W.; Attenkofer, K.; Jennings, G.; Smolentsev, G.; Soldatov, A. X-ray Snapshots for Metalloporphyrin Axial Ligation. *Chem. Sciences* **2010**, *1*, 642-650.

[40] Della-Longa, S.; Chen, L, X.; Frank, P.; Hayakawa, K.; Hatada, K.; Benfatto, M. Direct Deconvolution of Two-State Pump-Probe X-ray Absorption Spectra and the Structural Changes in a 100 ps Transient of Ni(II)-tetramesitylporphyrin. *Inorg. Chem.* **2009**, *48*, 3934-3942.

[41] Chen, L. X.; Zhang, X. Y.; Wasinger, E. C.; Attenkofer, K.; Jennings, G.; Muresan, A. Z.; Lindsey, J. S. Tracking Electrons and Atoms in a Photoexcited Metalloporphyrin by X-ray Transient Absorption Spectroscopy. *J. Am. Chem. Soc.* **2007**, *129*, 9616-9618.

[42] Chen, L. X.; Shaw, G. B.; Liu, T; Jennings, G.; Attenkofer, K. Exciplex Formation of Copper(II) Octaethylporphyrin Revealed by Pulsed X-rays. *Chem. Phys*. **2004**, *299*, 215-223.

[43] Chen, L. X.; Jager, W. J. H.; Jennings, G; Gosztola, D. J.; Munkholm, A.; Hessler, J. P. Capturing a Photoexcited Molecular Structure Through Time-domain X-ray Absorption Fine Structure. *Science* **2001**, *292*, 262-264.

[44] Chen, L. X.; Lee, P. L.; Gosztola, D.; Svec, W. A.; Montano, P. A.; Wasielewski, M. R. Time-Resolved X-ray Absorption Determination of Structural Changes following Photoinduced Electron Transfer within Bis-porphyrin Heme Protein Models. *J. Phys. Chem. B* **1999**, *103*, 3270-3274.

[45] Levantino, M.; Lemke, H. T.; Schiro, G.; Glownia, M.; Cupane, A.; Cammarata, M. Observing Heme Doming in Myoglobin with Femtosecond X-ray Absorption Spectroscopy. *Struc. Dyn.* **2015**, *2*, 04171.

[46] Levantino, M.; Schiro, G; Lemke, H. T.; Cottone, G.; Glownia, J. M.; Zhu, D. L.; Chollet, M.; Ihee, H. Cupane, A. Ultrafast Myoglobin Structural Dynamics Observed with an X-ray Free-electron Laser. *Nat. Commun*. **2015**, *6*, 6772.

[47] Mara, M.W.; Shelby, M.; Stickrath, A.; Harpham, M ; Huang, J. E.; Zhang, X. Y.; Hoffman, B. M.; Chen, L. X. Electronic and Nuclear Structural Snapshots in Ligand Dissociation and Recombination Processes of Iron Porphyrin in Solution: A Combined Optical/X-ray Approach. *J. Phys. Chem. B* **2013**, *117*, 14089-14098.

[48] Silatani, M.; Penfold, T. J. ; Rittmann, J.; Reinhard, M. E.; Rittmann-Frank, H. M.; Borca, C.; Grolimund, D.; Milne, C. J.; Chergui, M. *Proc. Nat. Acad. Sci.* USA **2015**, *112*, 12922-12927.

[49] Spaenig, F.; Ruppert, M. ; Dannhauser, J. ; Hirsch, A. ; Guldi, D. M. *Trans-2* Addition Pattern to Power Charge Transfer in Dendronized Metalloporphyrin C_{60} Conjugates. *J. Am. Chem. Soc.* **2009**, *131*, 9378-9388.

[50] Gouterman, M. A Theroy for the Triplet-Triplet Absorption Spectra of Porphyrins. J. *Chem. Phys.* **1960**, *33*, 1523-1529.

[51] Gust, D.; Moore, T. A. In The Porphyrin Handbook; Kadish, K. M.; Smith, K. M.; Guilard, R. Eds.; Academic Press: New-York, **2000**, 8, p153.

[52] Sano, M.; Komorita, S.; Yamatera, H. XANES Spectra of Copper(II) Complexes: Correlation of the Intensity of the 1s .fwdarw. 3d Transition and the Shape of the Complex. *Inorg Chem*. **1992**, *31*, 459-463.

[53] Tomson, N. C.; Williams, K. D.; Dai, X. L.; Sproules, S.; DeBeer, S.; Warren, T. H.; Wieghardt, K. Re-evaluating the Cu K Pre-edge XAS Transition in Complexes with Covalent Metal-ligand Interactions. *Chem. Sci.* **2015**, *6*, 2474-2487.

[54] Bianconi, A.; Dellariccia, M.; Durham, P.J.; Pendry, J. B. Multiple-scattering Resonances and Structural Effects in the X-ray-absorption Near-edge Spectra of Fe II and Fe III Hexacyanide Complexes. *Phys. Rev. B*. **1982**, *26*, 6502-6508.

[55] Bianconi, A.; Fritsch, E.; Calas, G.; Petiau, J. P. X-ray-absorption Near-edge Structure of *3d* Transition Elements in Tetrahedral Coordination: The Effect of Bond-Length Variation. *Phys. Rev. B.* **1985**, *32*, 4292-4295.

[56] Shadle, S. E.; Penner-Hanh, J. E.; Schugar, H. J.; Hedman, B.; Hodgson, K. O.; Solomon, E. I. X-ray Absorption Spectroscopic Studies of the Blue Copper Site: Metal and Ligand K-edge Studies to Probe the Origin of the EPR Hyperfine Splitting in Plastocyanin. *J. Am. Chem. Soc.* **1993**, 115, 767-776.

[57] Case, D. A.; Karplus, M. X.alpha. Multiple Scattering Calculations on Copper Porphine. *J. Am. Chem. Soc.* **1977**, *99*, 6182-6194.

[58] Bair, R. A.; Goddard, W. A. *Ab initio* Studies of the X-ray Absorption Edge in Copper Complexes. I. Atomic Cu^{2+} and Cu(II)Cl_2. *Phys. Rev. B* **1980**, *22*, 2667-2673.

[59] Kosugi, N.; Yokoyama, T.; Asakura, K.; Kuroda, H. Polarized Cu K-edge XANES of Square Planar $CuCl_4^{2-}$ ion. Experimental and Theoretical Evidence for Shake-down Phenomena. *Chem. Phys.* **1984**, *91*, 249-256.

[60] Chaboy, J.; Muñoz-Páez, A.; Carrera, F.; Merkling, P.; Sánchez Marcos, E. Ab initio X-ray Absorption Study of Copper *K*-edge XANES Spectra in Cu(II) Compouds. *Phys. Rev. B* **2005**, *71*, 134208.

[61] Yokoyama, T.; Kosugi, N.; Kuroda, H. Polarized Xanes Spectra of $CuCl_2 \cdot 2H_2O$. Further Evidence for Shake-down Phenomena. *Chem. Phys.* **1986**, *103*, 101-109.

[62] Spir, O; Simunek, A. Interpretation of Polarized Cu K X-ray Absorption Near-edge-structure Spectra of CuO. *J. Phys. Cond. Matter* **2001**, *13*, 8519-8525.

[63] Bocharov, S.; Kirchner, T.; Drager, G.; Sipr, O.; Simunek, A. Dipole and Quadrupole Contributions to Polarized Cu *K* X-ray Absorption Near-edge Structure Spectra of CuO. *Phys. Rev. B* **2001**, *63*, 045104.

[64] Choy, J. H.; Yoon, J.-B.; Jung, H. Polarization-Dependent X-ray Absorption Spectroscopic Study of $[Cu(cyclam)]^{2+}$-Intercalated Saponite. *J. Phys. Chem. B* **2002**, *106*, 11120-11126.

[65] Choy, J.-H.; Kim, D.-K.; Hwang, S.-H.; Demazeau, G. Cu *K*-edge X-ray-Absorption Spectroscopic Study on the Octahedrally Coordinated Trivalent Copper in the Perovskite-related Compounds $La_2Li_{0.5}Cu_{0.5}O_4$ and $LaCuO_3$. *Phys. Rev. B* **1994**, *50*, 16631-16639.

[66] Choy, J.-H.; Kim, D.-K.; Park, J.-C.; Choi, S.-N.; Kim, Y.-J. Intracrystalline and Electronic Structures of Copper(II) Complexes Stabilized in Two-Dimensional Aluminosilicate. *Inorg. Chem.* **1997**, *36*, 189-195.

[67] Kau, L. S.; Spira-Solomon, D. J.; Penner-Hahn, J. E.; Hodgson, K. O.; Solomon, E. I. X-ray Absorption Edge Determination of the Oxidation State and Coordination Number of Copper. Application to the Type 3 Site in Rhus Vernicifera Laccase and Its Reaction with Oxygen. *J. Am. Chem. Soc.* **1987**, *109*, 6433-6442.

[68] DeBeer, S.; Kiser, C. N.; Mines, G. A.; Richards, J. H.; Gray, H. B.; Solomon, E. I.; Hedman, B.; Hodgson, K. O. X-ray Absorption Spectra of the Oxidized and Reduced Forms of C112D Azurin from *Pseudomonas aeruginosa. Inorg. Chem*. **1999**, *38*, 433-438.

[69] Guldi, D. M.; Prato. M. Excited-state Properties of C_{60} Fullerene Derivatives. *Acc. Chem. Res*. **2000** *33*, 695-703.

[70] Zhang, X. Y.; Canton, S. E.; Smolentsev, G.; Wallentin, C. J.; Liu, Y. Z.; Kong, Q. Y.; Attenkofer, K.; Stickrath, A. B.; Mara, M. W.; Chen, et al. Highly Accurate Excited-State Structure of $[Os(bpy)_2dcbpy]^{2+}$ Determined by X-ray Transient Absorption Spectroscopy. *J. Am. Chem. Soc.* **2014**, *136*, 8804-8809.

[71] Zhang, X. Y.; Papai, M; Moller, K.B.; Zhang, J. X.; Canton, S. E. Characterizing the Solvated Structure of Photoexcited $[Os(terpy)_2]^{2+}$ with X-ray Transient Absorption Spectroscopy and DFT Calculation. *Molecules* **2016**, *21*, 235-243.

[72] Erler, B. S.; Scholz, W. F.; Lee, Y. J.; Scheidt, W. R.; Reed, C. A. Spin Coupling in Metalloporphyrin .pi.-cation Radicals. *J. Am. Chem. Soc.* **1987**, *109*, 2644-2652.

[73] Gans, P.; Buisson, G.; Duee, E.; Marchon, J. C.; Erler, B. S. Scholtz, W. F.; Reed, C. A. High-valent Iron Porphyrins: Synthesis, X-ray Structures, .pi.-cation Radical Formulation, and Notable Magnetic Properties of Chloro(meso-tetraphenylporphinato)iron(III) Hexachloroantimonate and Bis(perchlorato)(meso-tetraphenylporphinato)iron(III). *J. Am. Chem. Soc.* **1986**, *108*, 1223-1234.

[74] Lima, F. A.; Penfold, T. J.; van der Veen, R. M.; Reinhard, M.; Abela, R.; Tavernelli, I.; Rothlisberger, U.; Benfatto, M.; Milne, C. J.; Chergui, M. Photo-induced Dynamics of the Heme Centers in Cytochrome bc_1. *Phys. Chem. Chem. Phys.* **2015**, *17*, 2143-2151.

[75] Mitzner,R.; Rehanek, J.; Kern, J.; Gul, S ; Hattne, J.; Taguchi, T.; Alonso-Mori, R.; Tran, R. et al. L-Edge X-ray Absorption Spectroscopy of Dilute Systems Relevant to Metalloproteins Using an X-ray Free-Electron Laser. *J. Phys. Chem. Lett.* **2013**, *4*, 3641-3647.

[76] Hall, E.R.; Pollock, C. J; Bendix, J.; Collins, T. J.; Glatzel, P.; DeBeer, S. Valence-to-Core-Detected X-ray Absorption Spectroscopy: Targeting Ligand S. *J. Am. Chem. Soc.* **2014**, *136*, 10076-10084.

[77] Lundberg, M.; Kroll, S.; DeBeer, S.; Bergmann, U.; Wilson, S. A.; Glatzel, P.; Nordlund, D ; Hedman, B.; Hodgson, K. O.; Solomon, E. I. Metal-Ligand Covalency of Iron Complexes from High-Resolution Resonant Inelastic X-ray Scattering. *J. Am. Chem. Soc.* **2013**, *135*, 17121-17134.

[78] March, A. M.; Assefa, T.; Bressler, C. ; Doumy, G. ; Galler, A.; Gawelda, W.; Kanter, E. P.; Nemeth, Z.; Papai, M.; Southworth, et al. Feasibility of Valence-to-Core X-ray Emission Spectroscopy for Tracking Transient Species. *J. Phy. Chem. C.* **2015**, *119*, 14571-14578.

[79] Schreck, S. ; Beye, M. ; Fohlisch, A. Implications of Stimulated Resonant X-ray Scattering for Spectroscopy, Imaging, and Diffraction in the Regime from Soft to Hard X-rays. *J. Mod. Opt.* **2015**, *62*, S34-S45.

[80] Gel'mukhanov, F.; Salek, P.; Shalagin, A.; Agren, H. X-ray Raman Scatter under Pulsed Excitation. *J. Chem. Phys.* **2000**, *112*, 5593-5603.

[81] Wallin, S.; Monnereau, C.; Blart, E.; Gankou, J. R.; Odobel, F.; Hammarstrom, L. State-Selective Electron Transfer in an Unsymmetric Acceptor-Zn(II)porphyrin-Acceptor Triad: Toward a Controlled Directionality of Electron Transfer from the Porphyrin S_2 and S_1 States as a Basis for a Molecular Switch. *J. Phys. Chem. A* **2010**, *114*, 1709-1721.

[82] Petersson, J; Henderson, J.; Brown, A.; Hammarstrom, L.; Kubiak, C. P. Time-Resolved Electron Transfer in Porphyrin-Coordinated Ruthenium Dimers: From Mixed-Valence Dynamics to Hot Electron Transfer. *J. Phys. Chem. C* **2015**, *119*, 4479-4487.

[83] Pelado, B.; Abou-Chahine, F.; Calbo, J.; Caballero, R.; de la Cruz, P; Junquera-Hernandez, J. M.; Orti, E; Tkachenko, N. V.; Langa, F. Role of the Bridge in Photoinduced Electron Transfer in Porphyrin-Fullerene Dyads. *Chem.-Eur. J.* **2015**, *21*, 5814-5825.

[84] Kesti, T. J.; Tkachenko, N. V.; Vehmanen, V.; Yamada, H.; Imahori, H.; Fukuzumi, S.; Lemmetyinen, H. Exciplex Intermediates in Photoinduced Electron Transfer of Porphyrin−Fullerene Dyads. *J. Am. Chem. Soc.* **2002**, 124, 8067-8077.

[85] Niemi, M.; Tkachenko, N. V.; Efimov, A; Lehtivuori, H .; Ohkubo, K.; Fukuzumi, S.; Lemmetyinen, H**.** Exciplex Mediated Photoinduced Electron Transfer Reactions of Phthalocyanine-Fullerene. *J. Phys. Chem. A* **2008**, *112*, 6884-6892.

[86] Lehtivuori, H.; Lemmetyinen, H.; Tkachenko, N. V. Exciplex-Exciplex Energy Transfer and Annihilation in Solid Films of Porphyrin-Fullerene Dyads. *J. Am. Chem. Soc*. **2006**, *128*, 16036-16037.

[87] Gonzalez-Rodriguez, D.; Carbonell, E.; Rojas, G. D.; Castellanos, C. A.; Guldi, D. M.; Torres, T. Activating Multistep Charge-Transfer Process in Fullerene-Subphthalocyanine-Ferrocene Molecular Hybrids as a Function of π−π Orbital Overlap. *J. Am. Chem. Soc.* **2010**, *132*, 16488-16500.

TOC graphic